TEMPERATURE AND RATE DEPENDENT MODELLING OF MOLTEN THERMOPLASTIC ADVANCED COMPOSITES DURING FORMING

P. Harrison[1*] and N. Correia[2]

[1] School of Engineering, James Watt Building (South)
University of Glasgow, Glasgow G12 8QQ, UK
[2] Composite Materials and Structures Research, Institute of Mechanical Engineering and Industrial Management, Porto 4200-465, Portugal

* Philip Harrison (Philip.harrison@glasgow.ac.uk)
Keywords: *thermoforming, multi-scale modelling, shear characterisation*

1 Introduction

Biaxial advanced composites and engineering fabrics can be formed over complex doubly-curved geometries by virtue of their ability to undergo very large shear deformations. The shear compliance of the material is consequently an important factor in determining the stress distribution within the composite during forming. The fibrous nature of composites means that the transverse shear stiffness is very low and therefore the resistance to out-of-plane bending is also low. This means that very small compressive stresses within the forming sheet can often lead to undesirable defects such as out-of-plane wrinkling. These compressive stresses are usually eliminated through the use of a blank-holding system designed to induce tensile stresses within the sheet. The required amount of tensile stress therefore depends on the shear resistance of the forming sheet. Thus, it is clear that correct characterisation and modelling of this shear resistance is important if compressive stresses and the resulting defects are to be accurately predicted during forming.

Various types of shear behavior have been measured in continuous fibre reinforced materials: dry woven engineering fabrics have been demonstrated to show a strong coupling between their shear compliance and the in-plane tension acting along the fibre reinforcement [1, 2], non-crimp fabrics show a non-symmetric shear response in positive and negative shear due to the influence of the stitching [3-6] and the shear response of pre-impregnated advanced composites is strongly influenced by the liquid matrix phase, which is usually a molten thermoplastic polymer or an uncured thermosetting resin [7]. The fluid nature of the matrix means that the material is sometimes described as a fibre-reinforced fluid [8, 9]. Such materials have a rate-dependent viscoelastic shear response [10] resulting in an increase in the shear resistance with increasing shear strain rate. As the viscosity of the polymeric matrix phase is strongly temperature dependent, the shear resistance of the composite sheet is also temperature dependent. For thermosetting composites there can also be a time-dependence due to the increasing degree of cure of the polymer in time [11].

A significant body of work has been published on the topic of constitutive modelling of rate dependent advanced composites during the forming process. Some authors have implemented constitutive models based on ideal fibre reinforced fluid theory [12]. Alternatively a phenomenological approach can be used modelling the composite as a parent elastic sheet coupled together with a viscous fluid layer [13] or using various combinations of spring and dashpots elements [14-16]. All these approaches require experimental data in order to fit model parameters. Measuring the data experimentally can be a time consuming and costly undertaking, especially when considering both the rate and temperature dependence of these materials. Another difficulty is in correctly fitting the sometimes

numerous model parameters in order to accurately predict experimental shear test data, e.g. [17, 18]. A third strategy is to use homogenization methods to go from micro-scale predictions based on the matrix rheology, the fibre volume fraction and the fabric architecture to macro-scale forming predictions e.g. [19]. Using this approach and following on from previously work [7, 20-21], a 'Multi-Scale Energy Model' (MSEM) is used in here to predict the shear behaviour of advanced thermoplastic composites. These predictions are automatically incorporated into Finite Element (FE) simulations using an interface implemented within a material user-subroutine. The motives for such constituent-based predictive modelling are two-fold: (i) once the rheology is known the shear response of any composite comprised of matrix and continuous inextensible fibres can be predicted (ii) characterising the rheological behaviour of, for example, a thermoplastic matrix polymer at different shear rates and temperatures is relatively easy using modern rheometers, compared with the equivalent but more difficult task of characterising the rheology of textile composites using typical shear characterization tests [10, 18, 20, 22].

2 Finite Element Model

The FE model used in this investigation employs a similar strategy to that proposed by Cherouat and Billoët [14], namely a combination of truss elements, representing the high tensile stiffness fibres, and membrane elements, representing the shear properties of the viscous textile composite (see Figure 1). The truss elements employ a simple linear elastic material behaviour with a stiffness of 30 MPa (artificially low to reduce simulation times). The membrane elements have a shear resistance that, through an interface with a predetermined database of predicted shear stiffness behaviours, is selected during the forming simulation according to the angular shear rate within the element. This database is determined prior to the simulation using the MSEM, the latter is discussed in the following section.

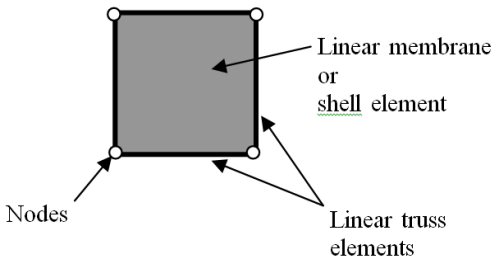

Figure 1. Mutually constrained truss and membrane (or shell) elements.

2 Multi-Scale Energy Model

The MSEM used in this work combines micromechanical models for the transverse and longitudinal viscosities of fibre reinforced fluids, with ideal fibre reinforced fluid theory and also with meso-scale observations of the tow shear kinematics within the composite sheet. Previously the tows within the sheet have been observed to shear at a lower rate than the average in-plane shear rate occurring across the sheet [e.g. 20, 22]. This results in energy losses due to friction between adjacent contacting layers of the composite. Various energy losses due to viscous friction during shear deformation, including the friction between adjacent layers, are calculated and used to obtain the overall shear-force resistance of the viscous composite. A detailed description of the MSEM is provided elsewhere [20]. As the predictions of the MSEM are directly related to the matrix rheology, they are both shear rate and temperature dependent. The predicted shear force data from the MSEM are fitted by polynomial functions. The coefficients of these functions are stored in a database and fed to the macro-scale constitutive shear model implemented in the membrane elements according to the angular shear rate in the membrane element.

3 Macro-scale Constitutive Shear Model

In this investigation a so-called 'Stress Power Model' (SPM) [7] is used to model the shear resistance of the membrane elements. The membrane elements are used both to produce shear resistance in the deforming sheet and accommodate contact during forming simulations. In the SPM, in-plane membrane shear stresses are related directly to

the shear-force of the composite sheet using two independent simultaneous equations. The first, Eq (1), is based on the assumption that the stress tensor is symmetric and can be obtained by rotating the in-plane stress tensor from its principal system (the system in which there are no shear stresses; for pure shear is the same as the orthogonal bisector system indicated by an orthogonal frame with its *x*-axis lying in the same plane as the two fibre directions and pointing in the direction that bisects the two fibre directions, denoted by $\hat{x}_b$ and $\hat{y}_b$ in Figure 2), to a system which has one of the fibre directions, i.e. $\hat{\mathbf{g}}_1$, co-linear with its x-axis

$$F_s = h_o \cdot \frac{\sin 2\phi}{2}\left(\tau_{xx} - \tau_{yy}\right) \tag{1}$$

where F_s is the shear force per unit length versus shear angle, θ, which can be approximated using a polynomial function of θ, i.e. $F_s(\theta)$. Also, $\phi = \left(\frac{\pi}{4} - \frac{\theta}{2}\right)$ is the rotation angle from the principal reference frame of the picture frame test to a frame with one of the tows aligned in the *x* direction (see Figure 2), τ_{xx} and τ_{yy} are the principal stresses of the extra stress tensor and h_o is the initial thickness of the sheet. Here, the model assumes the material is completely compressible, i.e. constant thickness with increasing shear angle. The second independent equation, Eq (2), is the stress power equation for a picture frame test [10]. Assuming no fibre stretching occurs

$$F_a \dot{d} = L_{PF}^2 h_o \cos\theta\left(\tau_{ij} D_{ji}\right) \tag{2}$$

where F_a is the axial force measured in a picture frame test, $\dot{d}$ is the axial displacement rate, τ_{ij} is the extra stress tensor and D_{ij} is the rate of deformation tensor and L_{PF} is the side length of the picture frame rig. It can be shown that

$$\tau_{xx} = \frac{F_s}{h_o}\left(\frac{\sin\theta - \cos^2\theta + 1}{\cos\theta \cdot \sin\theta}\right) \tag{3}$$

$$\tau_{yy} = -\frac{F_s}{h_o}\left(\frac{\sin\theta + \cos^2\theta - 1}{\cos\theta \cdot \sin\theta}\right) \tag{4}$$

By combining Eqs (1), (3) and (4), the shear stress can subsequently be expressed in an incremental form suitable for implementation in the Abaqus Explicit™ user subroutine, vumat. By adapting the transformations implemented by Yu in the original non-orthogonal constitutive model, e.g. [3], each stress increment is transformed from the fibre bisector system into the reference frame used by Abaqus (the 'updated' Green-Naghdi frame) before being added to the stress from the previous time step. The latter is also provided to the user subroutine in the 'current' or 'updated' Green-Naghdi system (i.e. the stress from the previous time step is rotated into the current Green-Naghdi frame).

$$\Delta\tau_{xx} = \frac{F_s^{n+1}}{h_o}\left(\frac{\sin(\theta+\Delta\theta) - \cos^2(\theta+\Delta\theta) + 1}{\cos(\theta+\Delta\theta)\cdot\sin(\theta+\Delta\theta)}\right) - \frac{F_s^{n}}{h_o}\left(\frac{\sin\theta - \cos^2\theta + 1}{\cos\theta\cdot\sin\theta}\right) \tag{5}$$

and

$$\Delta\tau_{yy} = -\frac{F_s^{n+1}}{h_o}\left(\frac{\sin(\theta+\Delta\theta) + \cos^2(\theta+\Delta\theta) - 1}{\cos(\theta+\Delta\theta)\cdot\sin(\theta+\Delta\theta)}\right) + \frac{F_s^{n}}{h_o}\left(\frac{\sin\theta + \cos^2\theta - 1}{\cos(\theta)\cdot\sin\theta}\right) \tag{6}$$

Here the superscript, *n*, indicates the angular shear rate using to fit the polynomial input curve, as will be explained in the following section.

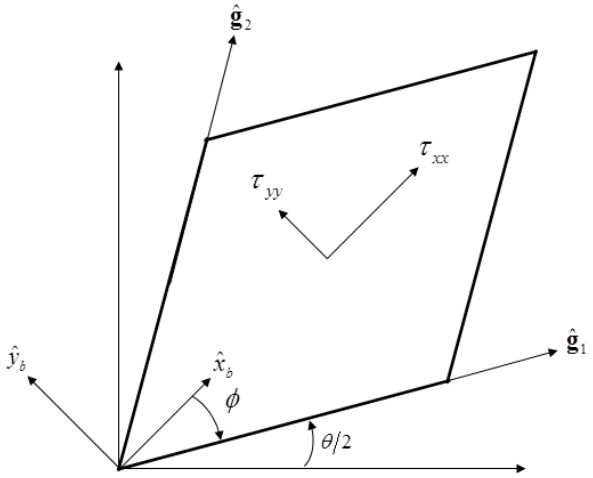

Figure 2. Reference systems used by the non-orthogonal constitutive model and the stress power model. $\hat{\mathbf{g}}_1$ and $\hat{\mathbf{g}}_2$ are covariant unit vectors that track the fibre directions (from [7]).

4 Interface for Rate Dependence

Implemented in the form described in Section 3, the model is a purely rate-independent model. However, by selecting F_s^n according to the shear rate of in the membrane element a rate dependent shear response can be generated, the algorithm to do this is described in detail in [7]. To illustrate, FE simulation predictions, incorporating the MSEM generated database of shear stiffness predictions are compared against bias extension and picture frame test results measured from a pre-consolidated glass/polypropylene textile composite (2x2 twill weave, fibre volume fraction = 0.35, thickness = 0.54 mm), the reader is referred to [20] for details of these experimental tests. Due to the kinematics of the picture frame shear test, an increasing average angular shear rate is imposed in the specimen as the shear angle increases whenever a constant displacement rate is imposed at the machine crosshead, as predicted by Eq (7)

$$\dot{\theta} = \frac{\dot{d}}{L_{PF}\sin\left(\frac{\pi}{4}-\frac{\theta}{2}\right)} \qquad (7)$$

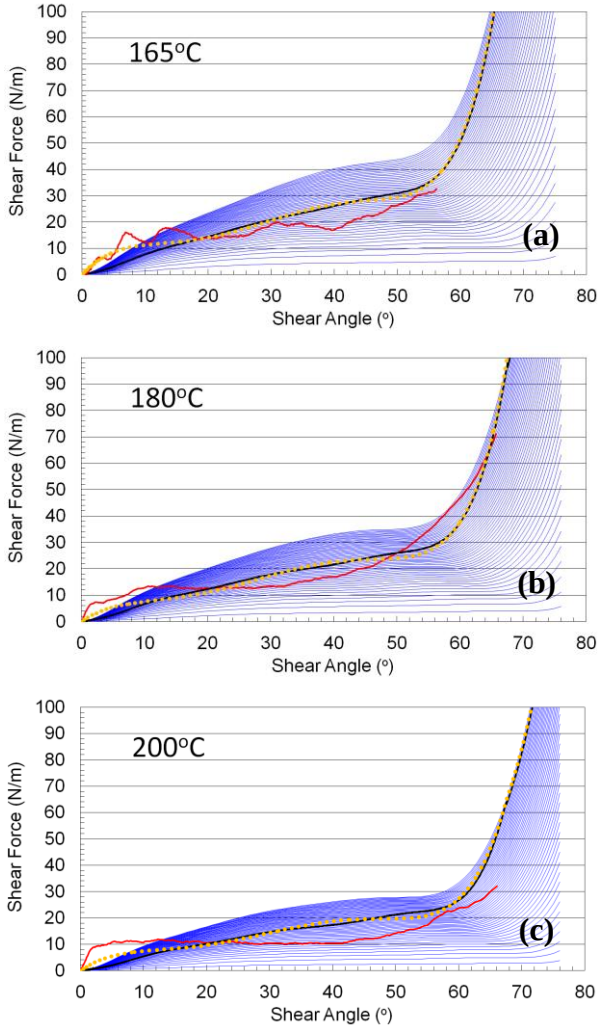

Figure 3. Shear force measurements from; (a) bias extension test at 165°C, (b) picture frame test at 180 °C and (c) picture frame test at 200°C tests, are shown by red lines [20]. Equivelent FE simulation predictions (black lines) generated using the database of polynomial input curves from the MSEM are also shown (blue lines) [20] (refer to section 4). FE simulation predictions created using polynomial input surfaces are also shown (dotted orange lines, refer to Section 5).

where $\dot{d}$ is the crosshead displacement rate and $\dot{\theta}$ is the angular velocity in the specimen. In contrast, the results of the MSEM are generated at constant angular velocities, the superscript, n on the polynomial function F_s^n indicates the angular shear rate used to fit F_s^n. In this instance, the MSEM predictions have been fitted by 11th order polynomial functions, one at each constant angular shear rate, at

progressively increasing angular shear rates ranging from 0.01 to 0.50 rads^{-1} in increments of 0.01 rads^{-1}, shown by the thin blue lines in Figure 3, hence *n* ranges from 1 to 50. The range of angular shear rates is selected to correspond to those occurring in the experimental tests.

By selecting the input shear force polynomial, F_s^n, according to the angular shear rate in the membrane element, the shear response of the element becomes rate dependent. If the angular shear rate in the element lies between the angular shear rates of neighbouring polynomials, then a simple linear interpolation is used to estimate the shear force between two curves. The method is demonstrated by the FE simulation prediction (the black line in Figure 3), which is produced by selecting polynomial input curves corresponding to the progressively higher shear rates imposed in the membrane elements. The simulation result (black line) consequently moves across the blue lines as the shear angle and angular velocity in the membrane element increases. The correspondence between the experimental results (red lines) and the simulation prediction (black line) is reasonably good in each of these tests. No artificial fitting parameters have been used to produce this correspondence, i.e. the result is predicted only from the matrix rheology, the fibre volume fraction, the fabric architecture and the observed meso-scale tow kinematics.

5 Interface for Rate and Temperature Dependence

This approach to modelling rate dependence, i.e. using multiple polynomial input curves, suggests a similar technique to modelling both rate and temperature dependence can be implemented. Take for example, the MSEM polynomial input curves shown in Figure 3 (for a temperature of 165^{o}C). Rather than fitting the data set with multiple polynomial curves using a distinct polynomial function for each angular shear rate, i.e. $F_s^n(\theta)$, the entire data set produced at a single temperature can be fitting using a single polynomial surface, i.e. $F_s(\theta,\dot{\theta})$, as shown in Figure 4. This process is facilitated by the surface fitting tool in Matlab^{TM} which allows polynomial surface functions of up to 5th order to be fitted. Weighting functions must be employed to ensure reasonable polynomials are produced. For example, in Figure 4 the fitted polynomial is seen to produce negative gradients for the lowest angular velocity data. By weighting the the low angular velocity MSEM predictions for the fitting procedure, the negative gradients can be eliminated from the fitted surface polynomial, this is important in achieving better convergence during forming simulations.

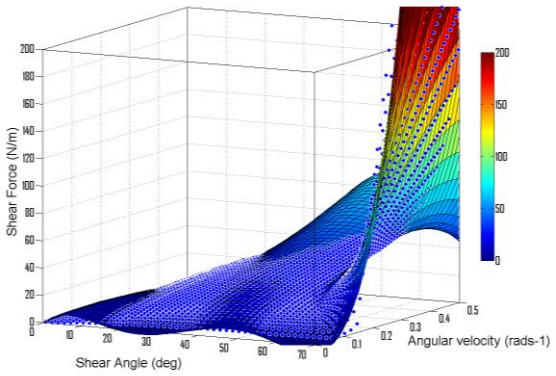

Figure 4. Polynomial surface, $F_s(\theta,\dot{\theta})$, fitted to the MSEM predictions (blue circles) made at 165^{o}C - shown previously in Figure 3.

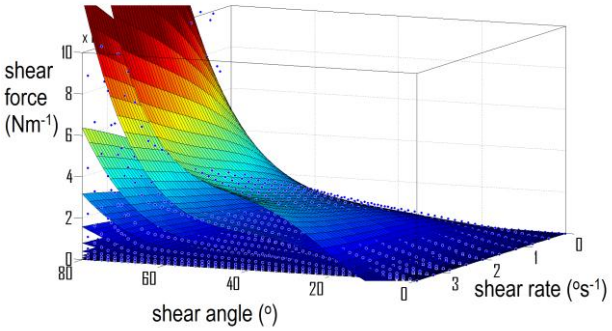

Figure 5. The shear force versus shear angle and shear rate predictions at several different temperature using the MSEM [20].

Distinct surface polynomials can be fitted to the MSEM predictions, with a different surface polynomial used for each different temperature, i.e. $F_s^m(\theta,\dot{\theta})$, in this case *m* is used to indicate the polynomial surface number corresponding to a given

constant temperature. For example, Figure 5 shows multiple surface polynomials fitted to the MSEM predictions. Analogous to the rate interface described in Section 4, linear interpolation has been used to calculate the shear stress if the element temperature lies between the distinct values used to generate the MSEM predictions.

Moving from the use of multiple polynomial input curves to a single polynomial input surface (for a constant temperature) results in a significant reduction in the number of polynomial coefficients stored in the material database. This could potentially affect the accuracy with which the surface polynomials can describe the exact form of the MSEM predictions. To test whether this loss of detail is significant, the picture frame simulations described in Section 4 were repeated, this time using an individual surface polynomial for each temperature. The results are shown by the orange dotted lines in Figure 3. Comparison of the predictions (black lines versus orange dotted lines) suggests that while some difference is introduced, the discrepancy is negligible.

By relating the temperature to the simulation time it is possible to model the effect of changing temperature on the shear force during a picture frame simulation. Various 'temperature versus shear angle' profiles (T1 to T3) imposed during 3 different picture frame simulations are shown in Figure 6a. The temperature is decreased from 200°C to lower values, twice over the course of each picture frame simulation (to 165, 135 and 133°C) in these non-isothermal simulations. The resulting 'shear force versus shear angle' predictions are shown in Figure 6b-d. Also shown are the shear responses predicted for constant temperatures of 165 and 200°C (taken from Figure 3a and 3c). In the first simulation the non-isothermal temperature follows profile T1 (dropping 35°C), producing the shear force result shown in Figure 6b (black dotted line). In the second simulation the non-isothermal temperature follows profile T2 (dropping 65°C) producing the shear force result shown in Figure 6c (black dotted line) and in the third simulation the non-isothermal temperature follows profile T3 (dropping 67°C) producing the shear force result shown in Figure 6c (black dotted line). It can be seen in Figures 6b and 6c that while the temperature remains above the polymer's crystallization temperature, T_c, changes in the polymer viscosity only have a limited effect on the composite's resistance to shear. Here a drop of 65°C, from 200°C, results in an approximate doubling of the shear force.

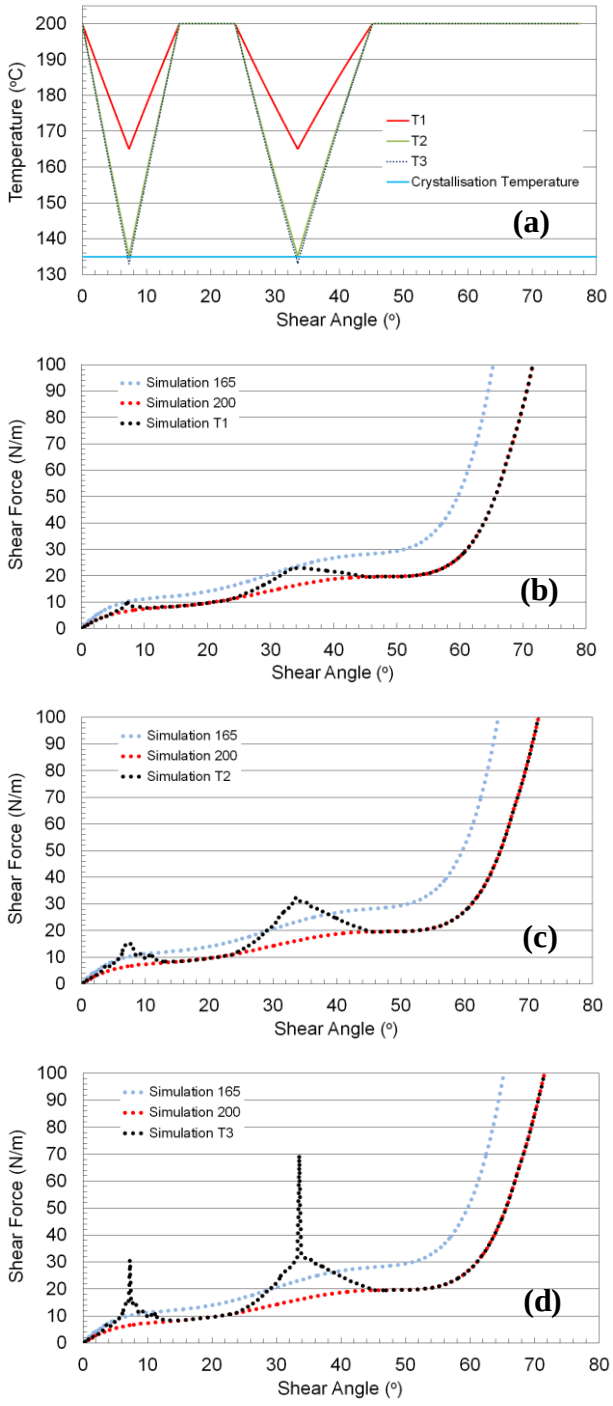

Figure 6. In (a) three different temperature profiles, T1, T2, and T3 are shown along with the crystallization temperature, T_c, at 135°C, (b-d) shear force versus shear

angle response when temperature profiles, T1, T2 and T3 are imposed during picture frame simulations.

For semi-crystalline polymers, T_c usually occurs between 10°C to 70°C lower than the polymer's melt-temperature, T_m, and the exact value depends on factors such as the rate of cooling and shear stress within the fluid [23]. Below T_c the viscosity rapidly increases, at a rate much faster than that measured above the melt temperature, i.e. the polymer begins to solidify.

The relationship between viscosity and temperature during crystallization is complicated but is nevertheless an important material property for accurate computational modeling of polymer processing, including injection-molding and thermoplastic composites forming processes [23]. In this investigation, because the T_m of polypropylene occurs at around 165°C, T_c is assumed to occur at 135°C. Note that this value has not been measured and is used in this investigation only as a plausible value with which to test the numerical implementation. The matrix viscosity is assumed to follow the viscosity-temperature relation as measured between 165 and 220°C [24], when extrapolated down to temperatures as low as 135°C. Below this temperature the shear stress in the sheet is assumed to increase more rapidly. Eq (8) has been implemented in the material user subroutine, vumat, in order to capture the effect of the increasing viscosity during solidification and the relation is imposed whenever the temperature, T, drops below T_c,

$$\tau_{12}^{T}(\theta,\dot{\theta}) = \tau_{12}^{T_c}(\theta,\dot{\theta}) e^{0.4(T_c - T)} \qquad (8)$$

here $\tau_{12}^{T}(\theta,\dot{\theta})$ is the shear stress at T (less than T_c) and $\tau_{12}^{T_c}(\theta,\dot{\theta})$ is the shear stress at T_c, which is a function of both the shear angle and shear rate, as determined by the MSEM. This relationship effectively causes the shear stress to increase by about 50 percent for every degree reduction in temperature below T_c. The effect of this behavior is shown in Figure 6d. Here the temperature profile follows T3. The solidifying composite shows a sharp increase in the shear force during picture frame simulations as the temperature falls momentarily by 2°C below T_c. Note, the main aim here is to test the implementation of the general method and further work is required to produce more realistic predictions based on physical measurements.

6. Benchmark Double Dome Forming Simulations: Sensitivity Study

The goal of this section is to further assess the likely effects of changing temperature on forming predictions using the benchmark double dome geometry [25] and to test the ability of the rate and temperature dependent SPM to cope with a rapidly falling temperature during the simulations. The same experiment as that described in [26] is modelled here though the material behavior used in these simulations is changed to that predicted by the MSEM for the pre-consolidated 2x2 twill weave, measured in [20] (see Section 5) rather than the glass/PP cross-ply laminate characterised in [26]. This change was prompted by uncertainty in the measured cross-ply laminate shear behavior; the straight fibres in a cross-ply laminate mean that picture frame test results are extremely sensitive to specimen misalignment, causing large scatter and consequently relatively unreliable data. Aside from this change, the FE simulation set-up is the same as that used in [26], i.e. using springs to induce tension in the blank, rather than a pressure blank-holder. The friction coefficient used in simulations for this investigation is 1.0. While this value seems high, peak friction values of up to 2.0 have been measured under conditions of low temperature, low pressure and high slip velocity, e.g. [27] and so this value is not considered to be unrealistic. The reader is referred to [26] for details on the simulation method. The maximum angular shear rate in the forming sheet can be estimated to be about $30^{o}s^{-1}$ (or $0.5rads^{-1}$), calculated from the experimental closure time of 0.74s+/-0.06s (error indicates standard deviation) and the shear angles predicted in the simulation. This corresponds well with the angular velocities imposed in the picture frame simulations (see Section 4).

Five simulations have been run, the first three at constant temperatures of 210°C (well above the melt temperature), 135°C (at the T_c implemented for this investigation) and 133°C (2°C below T_c). Two final

simulations, involving temperatures falling linearly from 210 to 135 °C and 210 to 133 °C have also been run. Notably the last simulation falls below T_c. The rapidly falling temperature is designed to approximate the drop one might expect to occur when the hot blank comes into contact with room temperature tooling. Vanclooster [27] calculated the cooling rate of a 2mm thick glass/PP advanced composite sheet initially at 195°C to be around 35°C during the first 0.75s following contact with aluminium tooling (held at 55°C). Thus, temperature drops of 75°C or 77°C over 0.75s are probably higher than might be expected when a 0.54mm thick glass/PP sheet comes into contact with room temperature tooling. However, the main goal here is to examine whether the code can accommodate falling temperatures (by selecting different input shear surfaces generated by the MSEM, see Figure 5) and to examine the effect on forming predictions when the sheet falls through T_c during the forming process. Two methods can be used to incorporate temperature changes in Abaqus Explicit™. One method is to use a fully coupled thermo-mechanical modeling strategy. Another is to link the temperature in the forming sheet to the simulation time, a method employed previously in [27]. The latter technique, which is employed in this investigation, is less accurate but computationally more efficient and simpler.

Figure 7 shows the results of the first three constant temperature forming simulations. In [26] it was observed that the localized regions of high shear predicted in the simulation (see for example the highlighted and zoomed region in Figure 7a) corresponded closely to defects produced in actual formed parts. When using a low coefficient of friction, i.e. 0.3, the degree of shear localization was found to increase significantly with increasing material shear stiffness (due to either lower blank temperature or higher forming rates). Increasing the friction coefficient reduced both the degree of shear localization and the latter's sensitivity to changes in the material shear resistance. In the current simulations, as the temperature is lowered to 135°C from 210°C the relatively high friction coefficient, i.e. 1.0, mitigates against a substantial increase in the degree of shear localization (compare Figures 7a and 7b), though it was noted that during the simulation conducted at 135°C, significantly more out-of-plane wrinkling occurred in the high shear regions and towards the perimeter of the sheet. These out-of-plane wrinkles were mostly eliminated due to increasing in-plane tension caused by the blank dragging across the surface of the female tool towards the end of the simulation.

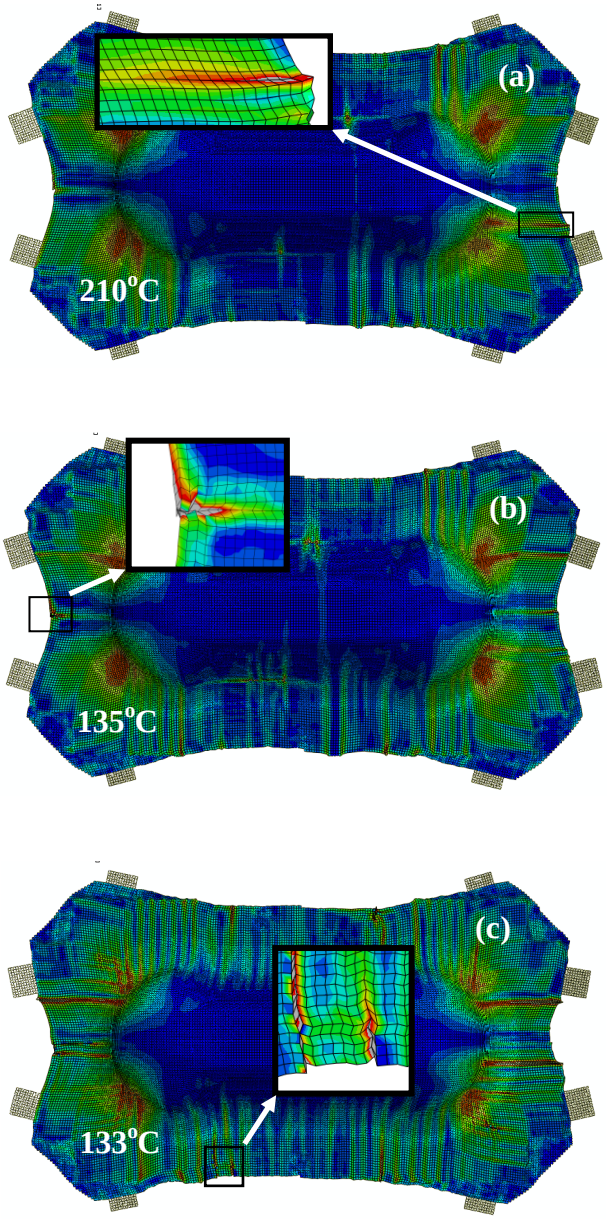

Figure 7. Forming simulation using the double-dome benchmark geometry at constant temperatures of: (a) 210°C, (b) 135°C and (c) 133°C.

The only notable differences between Figure 7a and 7b are: (i) more areas showing slightly sheared material in the central body of the formed part produced at the lower temperature and (ii) two of the out-of-plane wrinkles folded over at the end of the 135°C simulation to produce an alternative type of defect not seen at higher temperatures; these folded wrinkles remained at either end of the part. One of these folded wrinkles is highlighted in Figure 7b. Figure 7c shows the simulation result for 133°C, i.e. 2°C below T_c. The result is markedly different to both Figures 7a and 7b due to the significant increase in shear resistance, and shows a higher degree of localized shear and much more out-of-plane wrinkling during the simulation. Several of these wrinkles were severe enough to survive until the end of the forming step and were folded over at the edge of the formed part as the male and female tools closed together; one such example of a folder wrinkle is highlighted in Figure 7c. Figure 8 shows the same region as that highlighted in Figure 7c, from a side perspective, just prior to full closure of the tooling, i.e. at 96% of the total forming time; out-of-plane wrinkling is clearly visible. The form of the wrinkle is strongly influenced by the element size. Due to the modeling method, i.e. use of mutually constrained truss and membrane elements, the sheet has no resistance to out-of-plane bending and therefore represents a worse-case scenario in terms of the sheet's wrinkling response.

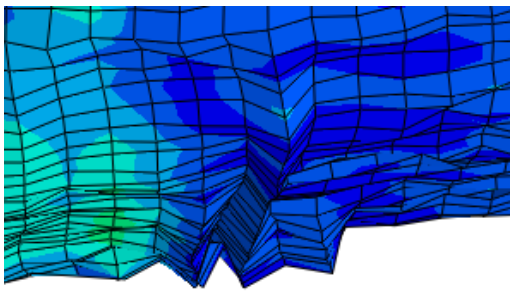

Figure 8. Form of out-of-plane wrinkle at position highlighted in Figure 7c just prior to full closure of tooling.

Figure 9 shows the final two simulations which involved linearly decreasing temperatures during the course of the forming step. Figures 9a and 9b involve temperature drops of 210 down to 135°C and from 210 down to 133°C respectively. As might be expected, the predictions obtained when a falling temperature is imposed, lie somewhere between the results produced when simulating the forming process at the temperature extremities. Figure 9a shows a result similar to that produced at 135°C though the degree of out-of-plane wrinkling and folding seen at the centre of the two ends of the formed part at 135°C (see Figure 7b) is reduced in Figure 9a. The highlighted region in Figure 9a can be compared with that in Figure 7b and shows less pronounced element distortion due to folding of the out-of-plane wrinkle. The result, in terms of the global shear deformation in the surrounding area, of a less pronounced out-of-plane wrinkle is a greater degree of in-plane shear localization in the regions adjacent to the wrinkle (compare Figures 9a and 7b). On the opposite end of the part shown in Figure 9a, the central wrinkle is no longer apparent when compared to Figure 7b. Again the result of eliminating the out-of-plane wrinkling appears to be a greater degree of in-plane shear localization towards the edge of the sheet in the surrounding area (compare Figure 9a and 7b).

Comparing Figure 9a and 9b, only slight differences are apparent. The central wrinkles are evident at both ends of the formed part in Figure 9b, as opposed to at just one end in Figure 9a suggesting slightly worse defects in Figure 9b, as might be expected. A much clearer difference is evident between Figures 7c and 9b with the former showing much more extensive in-plane localized shear and folding of out-of-plane wrinkles. This is to be expected and reflects the fact that the formed part of Figure 9b was at a higher temperature than the one of Figure 7c for the majority of the time during the forming process.

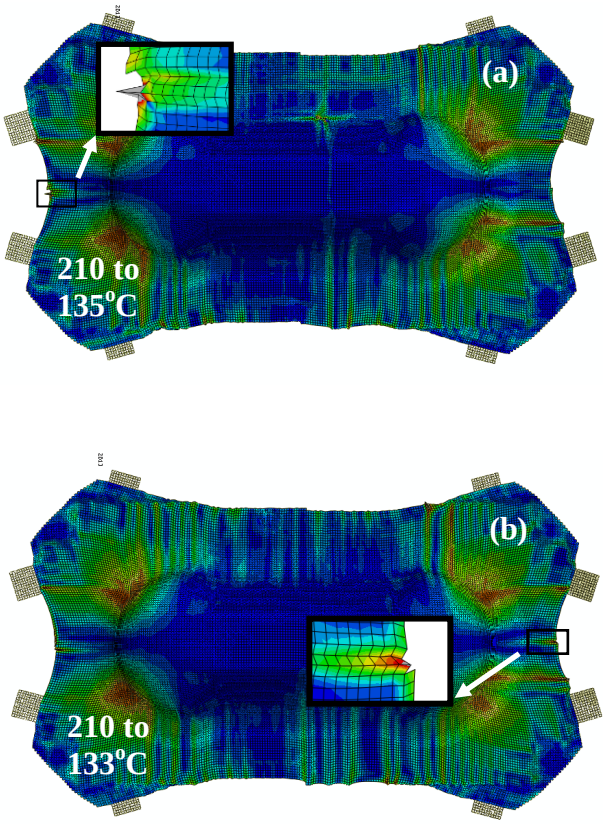

Figure 9. Forming simulation using the double-dome benchmark geometry while linearly decreasing the temperature from: (a) 210°C down to 135 °C and (b) 210°C down to 133°C.

7. Conclusions

The investigation presented in [26] and also the results of this work suggest several clear trends in the forming behavior of advanced thermoplastic composites. Increasing the friction coefficient reduces both the degree of shear localization and the latter's sensitivity to changes in the material's shear resistance, presumably due to greater in-plane tension induced in the sheet. If the friction coefficient is sufficiently low, then increasing the blank's in-plane shear stiffness (due to decreasing temperature and/or increasing shear strain rate) first of all causes an increase in the degree of in-plane shear localization across the sheet (the regions of localized shear have been shown to correspond to actual defects occurring in formed parts [26]). If the shear stiffness increases still further then at some point out-of-plane buckling and wrinkling of the forming sheet, that occur during the course of the simulation, becomes so severe that the wrinkles are no longer eliminated towards the end of the forming step by the rising in-plane tension generated by tool-ply friction. In these cases the wrinkle is folded over and pressed together as the gap between the male and female tools close. The presence of folded out-of-plane wrinkles appears to reduce the degree of in-plane shear localization in the surrounding region.

The simulations conducted in Section 4 and 6 demonstrate how both rate and temperature dependent behavior can be accurately modelled in characterization tests and forming simulations. The automated technique of passing shear force input surfaces generated by the MSEM, into the FE simulation, according to the values of state dependent variables within the vumat code (here both shear strain rate and temperature), allows fully predictive forming simulations to be conducted (i.e. based on the composite's matrix rheology, fibre volume fraction and fabric architecture). The FE forming simulations can predict not just global shear angle distributions across the formed part but also the severity and location of in-plane and out-of-plane wrinkling and buckles. It is not yet clear how important these defects are in terms of the part's final mechanical properties. Future work will involve the implementation of more accurate friction models and variable temperature distribution fields across the initial blank. The new method to incorporate both rate and temperature in the model will also permit the use of fully coupled thermo-mechanical simulations to enhance the accuracy of the forming predictions further still.

Acknowledgements

The authors wish to thanks the Royal Academy of Engineering for funding this work through a Global Research Award (ref. 10177/181) and also the Portuguese Agency for Innovation (agencia de inovação - adi) for funds provided through the projects Tooling Edge (FCOMP-01-0202-FEDER-003079 _NGHFT) and New Generation Hybrid Fuel Tank (FCOMP-01-0202-FEDER-013856 _ToolingEdge).

References

[1] J. Launay, G. Hivet, A.V. Duong and P. Boisse, Experimental analysis of the influence of tensions on in plane shear behaviour of woven composite reinforcements, *Comp. Sci. Tech.*, vol. 68, pp. 506–515, 2008

[2] P. Harrison, F. Abdiwi, Z. Guo, P. Potluri and W.R. Yu, Characterising the shear–tension coupling and wrinkling behaviour of woven engineering fabrics. *Comp. Part A*, vol. 43, no. 6, pp. 903-914, 2012

[3] W.R. Yu, P. Harrison and A.C. Long, Finite element forming simulation for non-crimp fabrics using a non-orthogonal constitutive equation, *Comp. Part A*, vol. 36, pp. 1079-1093, 2005

[4] S. Bel, N. Hamila, P. Boisse and F. Dumont, Finite element model for NCF composite reinforcement preforming: Importance of inter-ply sliding, *Comp. Part A*, 43, 2269–2277, 2012

[5] G. Creech and Pickett A.K., Meso-modelling of Non-Crimp Fabric composites for coupled drape and failure analysis, *J. Mater. Sci.*, vol. 41, pp. 6725-6736, 2006

[6] R.H.W. Thije ten and R. Akkerman, *Finite element simulation of draping with non-crimp fabrics*. 15th International Conference on Composite Materials, 27th June – 1st July Durban, South-Africa, 2005

[7] P. Harrison, W.R. Yu and A.C. Long, Rate Dependent Modelling of the Forming of Viscous Textile Composites, *Comp. Part A*, vol. 42, pp. 1719–1726, 2011

[8] T.G. Rogers, Rheological characterisation of anisotropic materials. *Composites*, vol. 20 no.1, pp. 21-27, 1989

[9] A.J.M. Spencer, Theory of fabric-reinforced viscous fluids, *Comp. Part A*, vol. 31, pp.1311-1321, 2000.

[10] G.B. McGuiness and C.M. O'Bradaigh, Characterisation of thermoplastic composite melts in rhombus-shear: the picture frame experiment. *Comp Part A*, vol. 29A, pp. 115-132, 1998

[11] C. Garschke, P.P. Parlevliet, C. Weimer and B.L. Fox. Cure kinetics and viscosity modelling of a high-performance epoxy resin film, *Polymer Testing*, vol. 32, no. 1, pp. 150–157, 2013

[12] E.A.D. Lamers, S. Wijskamp, and R. Akkerman, Drape Modelling of Multi-Layered Composites. *6th International ESAFORM Conference on Material Forming*, Salerno, 823-826, April 28-30th, 2003

[13] P. de Luca, P. Lefébure, A.K. Pickett, Numerical and experimental investigation of some press forming parameters of two fibre reinforced thermoplastics: APC2-AS4 and PEI-CETEX, *Comp. Part A*, vol. 29, no. 1–2, pp. 101-110, 1998

[14] A. Cherouat and J.L. Billoët Mechanical and numerical modelling of composite manufacturing processes deep-drawing and laying-up of thin pre-impregnated woven fabrics. *J. Mat. Proc. Tech.*, vol. 118, pp. 460-471, 2001

[15] S.B. Sharma and M.P.F. Sutcliffe, A simplified finite element model for draping of woven material. *Comp Part A*, vol. 35, no. 6, pp. 637-643, 2004

[16] A.A. Skordos, C. Monroy Aceves and M.P.F. Sutcliffe, A simplified rate dependent model of forming and wrinkling of pre-impregnated woven composites *Comp. Part A*, vol. 38, pp. 1318-1330, 2007

[17] X. Yu, L. Zhang, and Y.W. Mai, *Modelling and finite element treatment of intraply shearing of woven fabric*. International Manufacturing Conference in China (IMCC 2000) 16-17 August, Hong Kong, 2000

[18] A.S. Milani, and J.A. Nemes, An intelligent inverse method for characterisation of textile reinforced thermoplastic composites using a hyperelastic constitutive model, *Comp. Sci. Tech.*, vol. 64, pp. 1565-1576, 2004

[19] S.W. Hsiao, N. Kikuchi, Numerical analysis and optimal design of composite thermoforming process. *Computer Methods in Applied Mechanics and Engineering*, 177, 1–2, 1-34, 1999

[20] P. Harrison, M.J., Clifford, A.C. Long and C.D. Rudd, A constituent-based predictive approach to modelling the rheology of viscous textile composites, *Comp. Part A*, 38, 7-8, 915-931, 2004

[21] P. Harrison, W.R. Yu, J. Wang, T. Baillie, A.C. Long and M.J. Clifford, *Numerical Evaluation of a Rate Dependent Model for Viscous Textile Composites*, 15th International Conference on Composite Materials, 27 June -1st July, Durban, South Africa, 2005

[22] K. Potter, Bias extension measurements on cross-plied unidirectional prepreg. *Comp Part A*, 33, 63-73, 2002

[23] G.A. Mannella, V. La Carrubba, V. Brucato, W. Zoetelief and G. Haagh, No-flow temperature in injection molding simulation, *J. Appl. Poly. Sci.*, 119, 6, 3382–3392, 2011

[24] P. Harrison, M.J. Clifford, and A.C. Long, Constitutive modelling of impregnated continuous fibre reinforced composites micromechanical approach. *Plastics, Rubber and Composites*, vol. 31, no. 2, pp. 76-86, 2002

[25] http://www.wovencomposites.org/index.php, Woven Composites Benchmark Forum, 2008 (accessed 2nd June 2013)

[26] P. Harrison, R. Gomes and N. Correia, Press Forming A 0/90 Cross-Ply Advanced Thermoplastic Composite Using The Double-Dome Benchmark

Geometry, *Comp. Part A*, 2013 (submitted March 2013)

[27] K. Vanclooster, *Forming of Multilayered Fabric Reinforced Thermoplastic Composites*, PhD thesis, Catholic University of Leuven, 2010